Photochemistry and Photobiology, 2002, 75(4): 369–376

Estimation of Pedestrian Level UV Exposure Under Trees¶

Richard H. Grant*[1], Gordon M. Heisler[2] and Wei Gao[3]

[1]Department of Agronomy, Purdue University, W. Lafayette, IN;
[2]USDA Forest Service, Northeastern Research Station, 5 Moon Library, c/o State University of New York College of Environmental Science and Forestry, Syracuse, NY and
[3]USDA UVB Monitoring Program, Natural Resources and Ecology Laboratory, Colorado State University, Fort Collins, CO

Received 20 September 2001; accepted 7 January 2002

ABSTRACT

Trees influence the amount of solar UV radiation that reaches pedestrians. A three-dimensional model was developed to predict the ultraviolet-B (UV-B) irradiance fields in open-tree canopies where the spacing between trees is equal to or greater than the width of individual tree crowns. The model predicted the relative irradiance (fraction of above-canopy irradiance) under both sunlit and shaded conditions under clear skies with a mean bias error of less than 0.01 and a root mean square error of 0.07. Both model and measurements showed that the locations people typically perceive as shady, low-irradiance locations in the environment can actually have significant UV-B exposure (40–60% of that under direct sunlight). The relationship of tree cover in residential neighborhoods to erythemal UV-B exposure for children and adults was modeled for the 4 h around noon in June and July. Results showed that human exposures (on the horizontal) in cities located at 15 and 30° latitudes are nearly identical. For latitudes between 15 and 60°, ultraviolet protection factors (UPF) were less than 2 for less than 50% tree cover. A UPF of 10 was possible at all latitudes for tree cover of 90%.

¶Posted on the web site on January 28, 2002.

*To whom correspondence should be addressed at: Department of Agronomy, 1150 Lilly Hall, Purdue University, W. Lafayette, IN 47907-1150, USA. Fax: 765-496-2926; e-mail: rgrant@purdue.edu

Abbreviations: G, foliage projection area; I_{b0}, above-canopy direct beam radiation; I_{d0}, above-canopy diffuse radiation; I_{min}, minimum measured below-canopy irradiance; I_p, modeled below-canopy relative irradiance; I_r, measured below-canopy relative irradiance; I_0, above-canopy irradiance; M, tree cover fraction; MBE, mean bias error; MED, minimum erythemal dose, N, sky radiance distribution; P_o, probability of unobstructed direct beam radiation below canopy; P_o', probability of unobstructed diffuse radiation below canopy; PAR, photosynthetically active radiation; RMSE, root mean squared error; S, distance through the canopy; SPF, sun protection factor; SW, short-wave radiation; UPF, ultraviolet protection factor; UV, ultraviolet radiation; UV-A, ultraviolet-A radiation; UV-B, ultraviolet-B radiation; 3D, three-dimensional; θ, zenith angle; ρ, canopy vegetation density; ϕ, azimuth angle; Ω, direction of radiation.

© 2002 American Society for Photobiology 0031-8655/02 $5.00+0.00

INTRODUCTION

Solar ultraviolet radiation (UV) at the earth's surface has many implications for human health. Erythema is caused primarily by the ultraviolet-B (UV-B) portion of the solar spectrum (280–315 nm) and to a lesser extent by ultraviolet-A (UV-A) (315–400 nm). There appear to be complex relationships between skin cancers and sun exposure (1). Nonmelanoma skin cancers are thought to be correlated with cumulative lifetime UV exposure (2). Though medical opinions and epidemiological studies vary as to the relationship between sun exposure and cutaneous malignant melanoma (3), the statement that "it is now well established that sun exposure is one of the probable causes" is generally accepted by the research community (4). These health effects may be exacerbated by depletion of the stratospheric ozone layer and the attendant increases in UV radiation (5,6). Although changes in habits of recreation and dress, and the increased value placed on a "tan" are evidently largely to blame for most of the increases in skin cancer rates (7), these rates are expected to increase by approximately 2% for every persistent 1% loss in the average ozone concentration (5).

The human health impact of solar UV at the earth's surface depends on the environmental conditions as well as on human habits. Most people do not play out their lives in open fields but reside and work in environments in which there is significant obstruction to the sky and the direct sun by buildings and vegetation. Significant improvements in the prediction of open-environment exposure of surfaces at various slopes have been made in the past 10 years (8–10). Previous studies have shown that the relative irradiance (I_r) at pedestrian heights is significantly influenced by the canopies of vegetation and buildings (11–13). The influence of canopy structures on irradiance in open-tree canopies means that the canopy structure influences the UV exposure of people. The mean tree cover of medium-size cities in Texas, Ohio, California, Kansas, Alabama, New York, and Pennsylvania ranges from less than 10% to 37% (14,15). Because the climatic region, population density and socioeconomic characteristics of the population influence the tree canopy structure in urban areas, these factors also influence UV exposure. Rowntree (14) suggested that cities with more humid subtropical climates typically have greater tree canopy cover than those with northern continental climates, and cities with drier climates typically have less tree cover than those with

more moist climates (14). In a survey study of the tree cover of many cities, Nowak *et al.* (16) indicated that tree cover in residential areas ranges from 48% in forested climates to 27% in grassland climates and 11% in desert climates.

One approach to evaluating UV exposure on populations in different neighborhoods is to model the relative irradiance as influenced by trees and buildings and use the measured UV-B irradiance above the canopy to approximate the irradiance in pedestrian space under the canopy. The above-canopy UV-B irradiance measurements can be derived from monitoring networks such as that of the United States Department of Agriculture UV-B Radiation Monitoring Program (17). This paper describes the development and verification of a three-dimensional (3D) model for use in predicting the UV-B irradiance in open-tree canopies and applies the model to estimate UV-B exposure in residential suburban areas under cloud-free skies based on tree cover, latitude, day and time-of-day. The relative effectiveness of adding tree cover for the mitigation of erythemal UV-B exposure is also discussed.

METHODS

The model developed to predict UV-B irradiance within and below vegetation canopies is an adaptation of a 3D irradiance model by Gao *et al.* (18,19). The present model assesses the UV-B irradiance below canopies given the initial sky conditions and the canopy composition and structure. The canopy consists of a finite number of 3D geometrical bodies with the individual plant subcanopies (crowns) regarded as discrete scattering volumes of ellipsoidal shape. The model calculates the irradiance at a point in the array of crowns, with foliage in the crowns characterized by a single-foliage density (ρ) but with the possibility of defining individual crown dimensions.

The modeled below-canopy relative irradiance on a horizontal surface (I_p) was determined by the modeling of the probability of penetration of both diffuse radiation on a horizontal surface (I_{d0}) and direct beam radiation on a horizontal surface (I_{b0}) according to

$$I_p = \frac{(I_{b0} \times P_0) + (I_{d0} \times P_0')}{I_{b0} + I_{d0}} \tag{1}$$

where P_o is the probability that a direct beam of solar radiation ray will pass through the canopy unintercepted and P_o' the probability that sky diffuse radiation will pass through the crown unintercepted. The incident (above canopy) clear sky radiation was partitioned into diffuse sky and direct beam radiation according to the radiation models of Bird (20) for non-UV wavelengths and Shippnick and Green (21) for UV wavelengths.

The probability of a beam of radiation traveling unintercepted from the beam's source (inside or outside the canopy) to any given point in the array of subcanopies was defined as

$$P_o = e[^{-G(\Omega)\times\rho S}] \tag{2}$$

where Ω is the direction of radiation (with zenith angle θ and azimuth angle ϕ), $G(\Omega)$ the fraction of foliage area that is projected toward the source of radiation, ρ the foliage density (foliage area per unit canopy volume), and S the distance through the canopy that the ray must pass. This Poisson probability of penetration of direct beam radiation assumes that the leaves in each subcanopy are small and randomly dispersed. In our model the computation of the distance S that a ray passes through a discrete plant volume is calculated assuming all radiation sources to be on a reference plane above the canopy.

The probability of penetration of sky diffuse radiation is computed as

$$P_0' = \frac{\int_0^{2\pi}\int_0^{\pi/2} N(\varphi, \theta)\exp[-G(\theta)\rho S]\cos\theta \sin\theta \, d\theta \, d\varphi}{\int_0^{2\pi}\int_0^{\pi/2} N(\varphi, \theta)\cos\theta \sin\theta \, d\theta \, d\varphi} \tag{3}$$

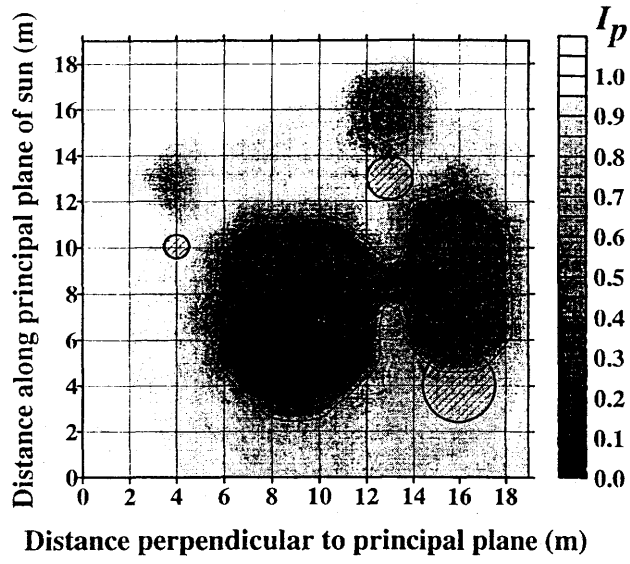

Figure 1. Example of modeled relative irradiance array. A plan view of the trees is indicated by the hatched circles. Darker shading corresponds with lower I_p values. The dark line in the shadow indicates the I_p = 0.5 level. The sunlight is coming from the bottom of the figure with a 30° zenith angle.

where N is the sky radiance for a given zenith angle θ and azimuth angle ϕ. The cloud-free sky radiance was modeled according to Harrison and Coombes (22) in the short-wave waveband (SW) (300–3000 nm), and Grant *et al.* in the photosynthetically active radiation (PAR) waveband (23) (400–700 nm) and in the UV-A and UV-B wavebands (24).

The model can also be used to estimate the irradiance within and below the vegetation canopies during partly cloudy and overcast days provided the diffuse fraction of the irradiance is known and the appropriate sky radiance distribution is used in Eq. 3. Sky radiance distributions are available for translucent overcast cloud cover in the SW (25), PAR (12), UV-A (26) and UV-B (26) wavebands and for opaque overcast sky conditions in the SW (27), and in the PAR (28), UV-A (28) and UV-B (28) wavebands.

Validation measurements. For model validation the vegetation density of the crown was set to a high value to effectively prevent penetration of radiation through the tree crown, and only cloud-free sky radiance distributions were used. Scattering was not included in the model because (1) there was only a small number of reflecting surfaces not associated with the single tree used in the validation measurements; (2) crown ρ was set to be opaque; and (3) reflections off the single tree were largely off shaded surfaces. The reflected energy off the shaded surfaces is small in the UV-A and UV-B because of the typically low (5–6%) leaf reflectance in the UV (29), and it is small in the PAR and SW because of the low amount of radiation available for reflection off the shaded surfaces resulting from the typically small diffuse fractions of cloud-free skies in the PAR and the SW. An example of the estimated I_p array for four trees under a cloud-free sky with solar zenith angle of 30° is illustrated in Fig. 1. Note that the pattern of shading of I_p by the individual crowns is relatively dispersed, with no distinct edges to the shadow. This is a result of the great influence of sky radiation on the UV-B irradiance.

The model was validated for use in open canopies typical of suburban backyard situations by comparing the model predictions with the minimum values of broadband irradiance measurements made under generally cloud-free skies during 17 measurement periods in the summers of 1996, 1997 and 1999 at West Lafayette, IN (40.5°N latitude) (Table 1). The measured relative irradiance (I_r) in or under the canopy was defined as

$$I_r = \frac{I_{min}}{I_0} \tag{4}$$

Table 1. Isolated tree measurement conditions

Date (d m y)	Distance from tree (m)	Direction to bole (deg)	Sky view factor	Mean solar zenith (deg)	Ozone column thickness (DU)	Total cloud fraction, type
31 May 96	0.3	271	0.05	56	315	0
31 May 96	1.5	278	0.17	64	315	0
31 May 96	4.9	259	0.40	43	315	0
3 July 96	3.7	274	0.47	59	315	0
3 July 96	3.7	276	0.47	60	315	0
27 May 99	4.3	220	0.55	20	341	0
27 May 99	4.3	290	0.55	38	341	0
3 July 96	5.5	278	0.61	63	315	0
27 May 99	4.9	220	0.61	28	341	0
27 May 99	4.9	290	0.61	45	341	0
31 May 99	6.7	257	0.67	41	315	0
31 July 97	5.5	180	0.69	23	291	0
3 July 96	8.2	277	0.71	62	315	0
5 Sept 97	7.9	180	0.75	34	269	0.3, Cirrus
18 Sept 97	9.1	195	0.78	30	288	0.3–0.4, Cirrus
29 Sept 97	9.1	175	0.78	46	265	0
29 Sept 97	11.6	242	0.84	63	265	0.2–0.3, Cirrus

where I_0 is the above-canopy irradiance and I_{min} the minimum measured irradiance at a height of 1.4 m below the canopy. Minimum values were chosen in the validation phase because the actual tree crown foliage density was not known, and the measurements were chosen in locations that did not appear to have sunflecks in the shadow pattern. Below-canopy irradiance sensors were in completely sunlit or completely shaded locations near a relatively isolated sweetgum (*Liquidambar styraciflua*) tree. A shaded location was defined as having canopy biomass between the sun and the sensor position so as to minimize the sunflecks on the sensors during the measurement period. The UV-B irradiance in a park-like grove was also measured to determine if the extrapolation of the single-tree model validation could also apply to a complex array of trees (Table 2). The grove consisted of large red oak (*Quercus rubra*), white ash (*Fraxinus americana*), red cedar (*Juniperus virginiana*) and red maple (*Acer rubrum*) trees approximately 30–40 m in height. The grove had a mean distance between trees of 13 m. The mean values of the measurements were used in this analysis. For both the single-tree and the grove measurements the above-canopy reference sensors were on a nearby building roof (with unobstructed view of the sky) within 150–300 m of the measurement locations.

The irradiance measurements were made in the four wavebands: SW, PAR, UV-A and UV-B. SW irradiance was measured using Kipp-Zonen CM5 radiometers (spectral response bandwidth of 320–2500 nm). The cosine response error of the CM5s was less than 1% for solar zenith angles less than 75°, and the temperature error was −0.15%/°C (30). The time constant of the sensor was approximately 4 s (31). PAR irradiance was measured using Li-COR 190SA sensors (LI-COR, Inc., Lincoln, NB) with a response bandwidth of 400–702 nm (32). The cosine response error of these sensors was less than 5% for solar zenith angles between 20 and 60° (32). UV-A irradiance was measured using SED038/UV-A/W sensors (International Light, Inc., Newbury, MA) with a spectral response of 314–388 nm (as reported by the manufacturer). The UV-A sensor system had a laboratory-measured temperature error of −0.5%/°C and a cosine response error of less than 10% for solar zenith angles between 20 and 80° (33). UV-B irradiance was measured using SED240/UV-B/W sensors (International Light) with a spectral response of 258–315 nm (as reported by the manufacturer). The UV-B sensor system had a laboratory-measured temperature error of −0.3%/°C and a cosine response error of less than 30% for solar zenith angles between 20 and 60° (33). The laboratory-measured time constant for the IL sensors was less than 5 s. In 1997 and 1999 the minimum erythemal dose (MED) (34) above the canopy was measured on the building roof (Table 1) using a UVB-1 sensor (Yankee Environmental Systems, Inc., Turners Falls, MA). This sensor had a spectral response bandwidth of 280–317 nm and a cosine response error of less than 10%. All sensors were sampled at 5–30 s intervals for between 30 min and several hours per location. The UVB-1 sensors were calibrated at the factory in September 1997 and July 1999. The UV-A and UV-B sensors were calibrated for a single wavelength at the factory in 1992 and 1993. The PAR sensors were calibrated at the factory in 1987. Because all the UV-B, UV-A, PAR and SW measurements were used ratiometrically (Eq. 4), the absolute calibration of the sensors was unimportant provided the sensor response was the same for a given irradiance. To assure equal response, all sensors were intercompared before each series of validation measurements and the recorded sensor response adjusted by linear least squares regressions to provide equivalent response during the validation measurements. Temperature response corrections were applied to the measurements before analysis. No corrections for the cosine response error of each sensor were applied because of the complexity of the shade environment. The lack of cosine correction likely resulted in overestimates of the relative UV-B irradiance and may have contributed to the estimated model error. Irradiance measurements for each waveband were normalized by the measured flux density at the above-canopy reference location.

Table 2. Tree grove measurement conditions

Date (d m y)	Sky view factor	Solar zenith median (deg)	Ozone column thickness (DU)	Total cloud fraction, type
18 June 99	0.57	49	377	0.2, Cirrus
18 June 99	0.13	42	377	0.1, Cirrus
18 June 99	0.57	49	377	0.2, Cirrus
18 June 99	0.13	42	377	0.1, Cirrus
7 July 99	0.13	22	309	0.1, Cirrus
7 July 99	0.10	34	309	0.1, Cirrus
7 July 99	0.66	29	309	0.1, Cirrus
7 July 99	0.25	26	309	0.1, Cirrus
7 July 99	0.13	18	309	0.1, Cirrus

Upward-facing hemispherical photographs from each measurement site were made using a Canon 7.5 mm lens. The photographs were analyzed to determine the total sky obscuration caused by canopies for each 10° annulus, either by a grid of fine lines with 10° intervals in both azimuthal and zenithal directions or by analyzing digitized images of the photographs using Glic v2.0 developed by C. Canham (Institute of Ecosystem Studies, Millbrook, NY). In the manual analysis of photographs an area of the sky hemisphere was defined as obscured if the sky was not visible at the intersection of the azimuthal and zenithal grid lines. In the digital analysis of the photographs each pixel was evaluated for sky obscuration or visibility. The sky view for the below-canopy measurement locations varied from 0.05 to 0.84 for measurements made near a single tree (Table 1) and from 0.10 to 0.66 for measurements made in the tree grove (Table 2).

Model application. The model was used to predict the relative UV-B exposure for various surfaces on a person randomly moving around in a tree-covered park near three major metropolitan areas of the United States of America. The relative exposure on a person in the park was estimated from the areal average I_p across a regular distributed 11 × 11 array of spherical trees with the cover fraction equivalent to the literature values. The I_p value over a range of solar zenith angles was determined for cloud-free sky conditions, calculated at the height of the crown base (assumed pedestrian height) for a regular array of spherical crowns.

One objective of the project was to provide a means to estimate UV-B exposure based on weather information and satellite or aircraft images of the area. To link the tree cover interpreted from the imagery to the sky view from the ground, the model was run for the 11 × 11 array of opaque spherical tree crowns assuming an isotropic sky radiance distribution so that the diffuse irradiance fraction is equivalent to the sky view factor. The mean sky view initially decreased rapidly with increasing tree cover until approximately

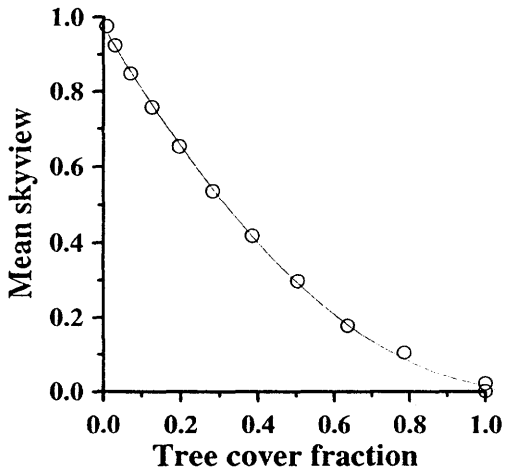

Figure 2. Modeled relationship between tree cover and sky view.

50% cover and then decreased more gradually with continued increase in the tree cover (Fig. 2). The tree cover fraction and solar zenith angle were then regressed against the areal average I_p to provide a means to relate below-canopy irradiance and exposure to above-canopy irradiance and exposure for locations at a given latitude on a given day and time. The relationship between the canopy cover fraction (the area of the ground divided by the area of canopy covering the ground by looking downwards into the canopy from directly overhead) and the sky view (a weighted area of sky visible from the ground when looking upwards through the canopy) was determined by setting the sky radiance function to a constant value and noting the diffuse-only relative irradiance.

Estimates of exposure on people within the tree array were made for the 10.00 A.M. to 2.00 P.M. interval (Eastern Standard Time) over the summer period of June through July at latitudes of 15, 30, 45 and 60°. The densities of the tree array were chosen to produce tree cover fractions of 0.1, 0.3, 0.5, 0.7 and 0.9. The areal average I_p for a given solar zenith angle and tree cover fraction provided the relationship between the above- and the below-canopy irradiance for the tree array. The relationship between solar zenith and cloud-free sky erythemal UV-B (34) was based on an irradiance by solar zenith angle regression of the UVB-1 irradiance measurements for 22 June 2000 (ozone column of 274 DU; EarthProbe TOMS V.7 Archive Overpass data, http://jwocky.gsfc.nasa.gov/) from the USDA UV-B Radiation Monitoring Program network sites at Mauna Loa, HI (elevation 3397 m, latitude 19.5°). The measured erythemal UV-B values were adjusted to sea level using the mean ratio of sea level to 3400 m modeled irradiance (0.857) based on the Schippnick and Green model (21). The cumulative daily exposure for the 4 h period centered on solar noon was described using the MED defined by Parrish *et al.* (35). An MED is the erythemally weighted amount of UV radiation (201 J/m^2) that will cause an erythemal response in light-skinned people.

RESULTS AND DISCUSSION

Model accuracy

The accuracy of the model to predict near-surface irradiance in the vicinity of a single tree was evaluated by comparing I_p with measured I_r for all four wavebands. In general, the modeled values were greater than the measured values. However, the variable density of the tree crown and the deviation of the tree crown shape from the modeled ellipsoid resulted in a larger fraction of sky penetrating through the oddly shaped crown and making the measured values sometimes greater than the modeled values. The mean bias error (MBE) of the model was 0.026, whereas the root mean

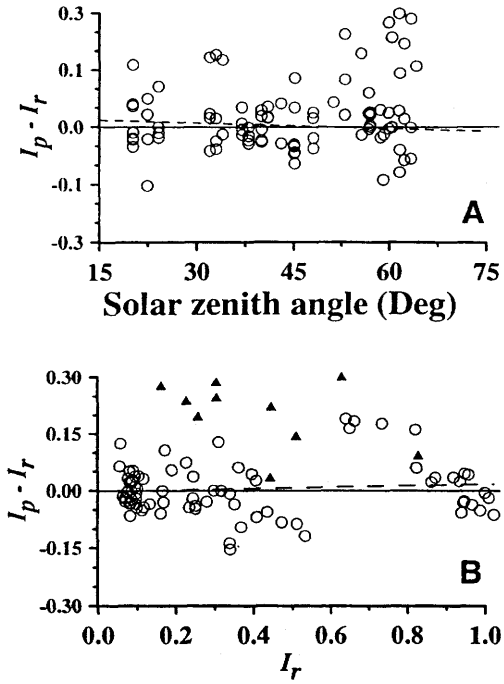

Figure 3. Model accuracy—Panel A illustrates the relationship of model error to solar zenith angle for measurements made near the single tree. Panel B illustrates the relationship of the model error to the magnitude of the measured relative irradiance, with errors for periods when the solar zenith angle was less than 55° (open circles) and greater than 55° (filled triangles). Dashed lines represent the linear regression of the error on solar zenith angle.

squared error (RMSE) was 0.093 (n = 92). The model error was relatively insensitive to the magnitude of the measured I_r (Fig. 3). This is similar to the model accuracy reported by Gao *et al.* (18), although the measured values used in their analysis were the mean values and not the minimum values used here. Gao *et al.* found that the model had MBE of 0.038 and 0.033 for apple orchard and maize canopies, respectively (18). The model RMSE was 0.082 and 0.061 for the apple orchard and maize canopies, respectively (18).

The modeled I_p tended to overestimate the measured I_r at high solar zenith angles. This was partly because of the decreasing ratio of direct beam to diffuse sky radiation with increasing solar zenith angle and partly because of the inability to correctly adjust the measured UV-B values for the sensor cosine response error in the shade. The impact of not being able to correct the measurements for noncosine response was minimized by excluding the measured UV-B values when the solar zenith angle was greater than 55° (33) (values indicated by the filled triangles in Fig. 3B). Excluding these measurements from the estimation of model accuracy reduced the model MBE for the single-tree measurements to 0.004 and increased the RMSE slightly to 0.068 (n = 82).

Areal mean I_p estimation

The areal mean I_p under the 11 × 11 regular array of spherical trees was determined for a range of solar zenith angles and tree cover fractions (Fig. 4). In general, the higher the

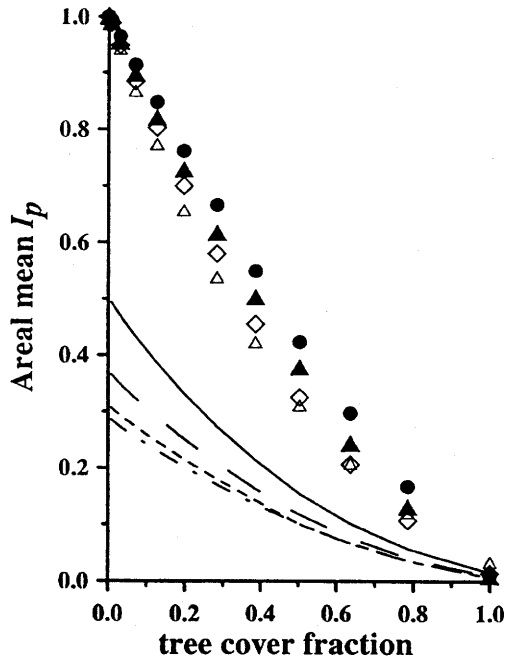

Figure 4. Modeled relative irradiance for the 11 × 11 tree array. The areal mean relative irradiance across the entire array for solar zenith angles of 15° (filled circle), 30° (filled triangle), 45° (open diamond) and 60° (open triangle) and the areal mean relative irradiance in the shade across the array for solar zenith angles of 15° (dash–dot line), 30° (dashed line), 45° (long dashed line) and 60° (solid line) are indicated.

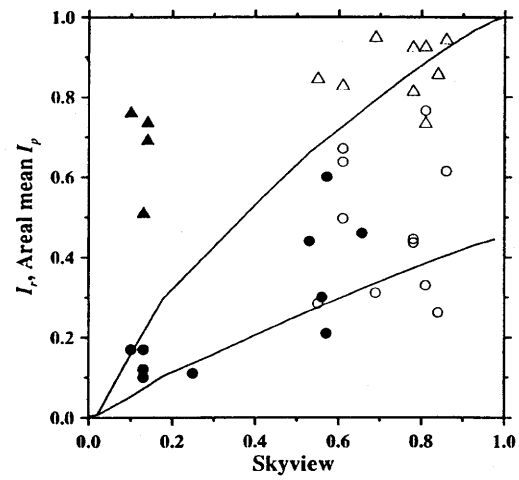

Figure 5. Comparative measurements and modeled relative UV-B irradiance. Measured relative irradiance of shaded (open circles) and sunlit (open triangles) locations near the single tree and shaded (filled circles) and sunlit locations (filled triangles) in the tree grove are indicated. The solid lines represent the domain between the modeled areal mean relative irradiance for both shaded and sunlit regions (upper curve) and the areal mean relative irradiance of only the shaded regions (lower curve) in the 11 × 11 array of trees for a solar zenith angle of 15°.

solar zenith angle, the closer the mean areal relative irradiance for a given tree cover fraction approached 1/(tree cover fraction). The rate of change in mean areal relative irradiance with change in tree cover was greatest at low tree cover fractions and least at high fractions.

The exposure received by pedestrians in the treed area was estimated by using a time history of UV-B monitoring measurements from the USDA UVB Monitoring Network (17). By associating the view factor with the canopy cover, the areal mean exposure of people in vegetated locations can be estimated based on remotely sensed tree cover. The validity of this approach of estimating exposure based on tree cover for a canopy of trees was evaluated by comparison of the modeled minimum and maximum values with the mean values measured in the grove of trees, which were distributed irregularly across the landscape. The modeled mean areal I_p was then compared with the measured relative irradiance in the tree grove for specific sunlit and shaded sensor locations. Figure 5 illustrates the individual I_r values relative to the mean areal I_p for shaded and sunlit areas for the grid of regularly distributed spherical trees using the relationship between sky view (measured) and tree cover fraction (modeled). In general, shaded environments with small sky view had the lowest relative irradiance. Areas near the single tree had I_r values of 0.5–0.3 (Fig. 5) corresponding to an equivalent ultraviolet protection factor (UPF) (analogous to the sun protection factor [SPF] used to describe sunscreen protection) of 2–3. Clearly, significant exposure of pedestrians is likely unless the tree cover has a nearly closed canopy. The advantage of being in the shade appears to decrease with increasing solar zenith angle; however, it should be noted that the MED at the higher solar zenith decreases to approximately 2 MED/h when the solar zenith angle increases to 45° (Table 1). Results showed that the envelope representing the areal mean minimum (shade) I_p for solar zenith angles ranging from 15 to 60° approximated the mean of the observed values in the grove of trees as well as near the single tree (Fig. 3). Values well above the shade areal mean I_p were in direct sunlight. Variations around the areal mean shade I_p are expected because point and area averages are being compared.

The multivariate regression of the mean areal I_p of the 11 × 11 array of trees for solar zenith angles of 15, 30, 45 and 60° against the calculated tree cover fraction and solar zenith angle resulted in the relationship:

$$I_p = -0.431 + 1.5787\, e^{-M} - 0.0435 \ln(\theta) \qquad (5)$$

where M is the tree cover fraction and θ is the solar zenith (adjusted $r^2 = 0.97$). In general, I_p decreased with solar zenith angle and increased with tree density.

Exposure estimation for residential areas

UV exposure during childhood is a risk factor in the development of skin cancers in adults (3). Reducing the exposure of children and young adults should therefore reduce the risk of later-life cancers. Studies have shown that children in primary grades may receive greater UV exposure than those in secondary grades (36). Diffey *et al.* (36) attributed this difference in exposure to young children spending more time playing outdoors in open areas. The exposure of children to UV-B between 10.00 A.M. and 2.00 P.M. during the summer period of June and July was estimated at four latitudes and six tree cover fractions. Because the above-canopy irradiance for all simulations was only a function of the solar

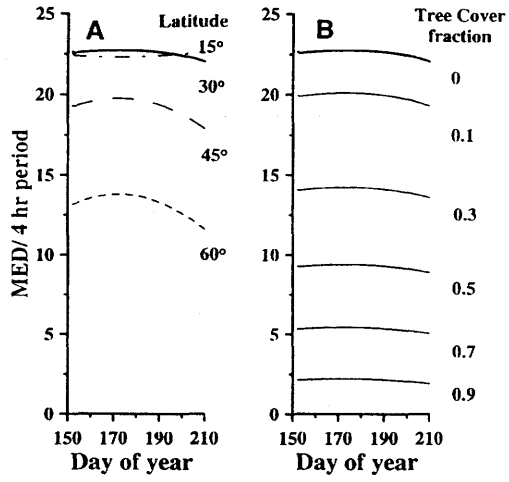

Figure 6. Estimated erythemal UV-B exposure for midday exposures during June and July. Panel A illustrates the daily exposure above canopy for locations at four different latitudes. Panel B illustrates the daily exposure for varying tree cover fractions at latitude 30°.

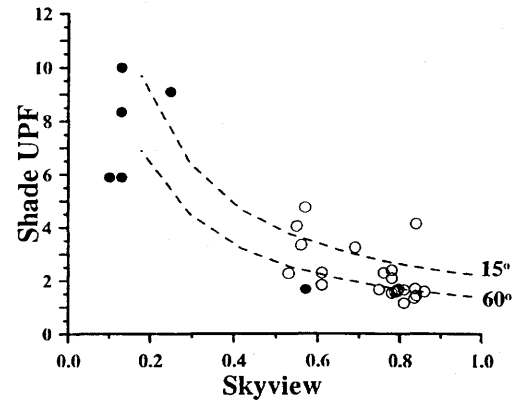

Figure 7. UPF for shaded environments—Measured UPF values from the single tree (open circles) and tree grove (filled circles) are indicated. The mean shade UPF for the 11 × 11 tree array under solar zenith angles of 15 and 60° are indicated by the dashed lines.

zenith angle, the variation in the daily exposure at each latitude location was a result of the combined effect of latitude and canopy cover.

The estimated daily exposure for a child playing under clear skies during the 4 h centered around solar noon varied from approximately 12 ± 0.8 MED for cities at 60° latitude to 22 ± 1.5 MED for cities at 15 and 30° latitudes (Fig. 6A). The similarity in exposure between cities at 15 and 30° latitudes was because of the time of year chosen for the comparison (solar declinations of approximately 20°). The maximum MED for a given day was at the summer solstice for latitudes above 23.5°, whereas the exposure at 15° latitude was nearly constant throughout the period (Fig. 6A).

Increasing tree cover decreases exposure. The equivalent mean UPF of tree cover was less than 2 for tree cover of less than 0.5 at all latitudes (Table 3). The nonlinearity of the error in mean UPF indicated in Table 3 is a result of UPF being equal to $1/(I_p \pm 0.07)$. The undefined errors in the table are a result of mean $I_p < 0.07$. Mean UPF values greater than 5 typically required tree cover of greater than 0.7, a relatively dense canopy. The corresponding relationship between UPF and sky view (related to tree cover by Fig. 4) for shaded locations in the simulated 11 × 11 tree array illustrates the range of approximately 2 SPF units for solar zenith angles ranging from 15 to 60° (Fig. 7). Although high tree cover minimizes the areal mean UV-B exposure and maximizes the areal mean UPF, a careful choice of locations within an array of trees can result in high UPF while the tree cover is low. Maximum benefits of any given tree cover can be had by minimizing the view of the sky by being in the shade and near individual trees of the array. Grant (11) showed that greater protection (UPF of 10) could be had by people if they stay under the tree crowns. This corresponds with the UPF associated with most of the measurements made in the tree grove (Fig. 7). The range of UPF values evident for a given sky view is the result of measurements being made under a range of solar zenith angles at similar locations in the vicinity of the single tree and in the tree grove. It should be remembered that the model reported here estimates the exposure on horizontal surfaces, whereas receptor surfaces on the human body have a wide range of orientations. The estimates described here would apply only to an exposed vertex of the head. Exposure to the face can be estimated using corrections for various orientations of the head and various parts of the head developed by Kimlin and Parisi (37) and others.

One limitation of this approach is the limited availability of UV-B irradiance measurements within urban areas. This is important because the UV-B irradiance within urban areas can be expected to differ from that of the surrounding rural area because of differences in the ground albedo and air pollution (38,39). As such, estimates of UV-B exposure on people in cities should be based on urban UV-B measure-

Table 3. Mean modeled UPF for varying tree cover

Latitude	Tree cover fraction 0.1	0.3	0.5	0.7	0.9
15	1.4 ± 0.1*	1.6 ± 0.2	2.4 + 0.4/−0.5	4.2 + 1.8/−1.1	10.6 + 30.5/−4.5
30	1.4 ± 0.1	1.6 ± 0.2	2.4 + 0.4/−0.5	4.2 + 1.8/−1.1	10.6 + 30.5/−4.5
45	1.2 ± 0.1	1.7 ± 0.2	2.6 + 0.6/−0.4	4.7 + 2.3/−1.2	14.6 + UND†/−7.4
60	1.2 ± 0.1	1.7 ± 0.2	2.7 + 0.6/−0.4	5.2 + 3.0/−1.4	19.7 + UND/−11.4

*± Values based on RMSE model error of 0.07.
†UND = undefined.

Table 4. Relative benefit of tree cover to mean erythemal UV-B exposure (change in exposure/change in tree cover fraction)

	Tree cover fraction				
Latitude	0.1	0.3	0.5	0.7	0.9
15	1.19	1.26	1.18	1.09	1.00
30	1.19	1.26	1.18	1.09	1.00
45	1.45	1.35	1.23	1.13	1.03
60	1.62	1.40	1.27	1.15	1.05

ments (39). This is an important area for development because only a few cities in the United States have UV-B monitoring under way.

We have considered here only the UV-B exposure under clear skies resulting from the existing vegetation cover. From an urban landscape planning point of view, how much tree cover is best to reduce UV-B exposure on pedestrians? Although obviously the increase in tree cover always decreases the exposure to UV-B (Fig. 6B), the change from no tree cover to 0.1 tree cover has a greater impact than the change from 0.9 to 1.0 cover. Therefore, planting some trees in an open area creates real sun protection benefits. Because of the interplay of tree cover on sky view, there is an optimal value where the effect of additional tree cover in reducing exposure is the greatest. The relative effectiveness of planting trees to increase tree cover and reduce erythemal UV-B exposure on pedestrians was evaluated by comparing the fractional change in exposure over the 2 month exposure period with the fraction of tree cover. Model results indicate that cities with low latitudes of 15–30° receive the maximum benefit of tree cover relative to UV-B exposure when the tree cover fraction is approximately 0.3 (Table 4). For any given tree cover fraction, the greatest benefits of increasing tree cover to mitigate UV-B exposure occur at high latitudes (Table 4).

Acknowledgements—This study was funded in part by the U.S. Forest Service and it's Northern Global Change Research Program under cooperative agreement 23-793 of the Northeastern Research Station and in part by the Purdue Experiment Station and is journal paper number 16699 of the Station.

REFERENCES

1. Vitasa, B. C., H. R. Taylor, P. T. Strickland, F. S. Rosenthal, S. West, H. Abbey, N. G. Sk, B. Munoz, and E. A. Emmett (1990) Association of nonmelanoma skin cancer and actinic keratosis with cumulative solar ultraviolet exposure in Maryland watermen. *Cancer* **65**, 2811–2817.
2. Lloyd, S. A., E. S. Im and D. E. Anderson Jr. (1993) Modeling the latitude-dependent increase in non-melanoma skin cancer incidence as a consequence of stratospheric ozone depletion. In *Stratospheric Ozone Depletion/UV-B Radiation in the Biosphere* (Edited by R. Hilton Biggs and E. B. Joyner Margaret), NATO ASI Series I, Vol. 18, pp. 329–337. Springer-Verlag, New York.
3. Heisler, G. M. and R. H. Grant (2000) *Ultraviolet Radiation, Human Health, and the Urban Forest. U.S. Dept. of Agric. Gen. Tech. Rep. NE-268.* U.S. Department of Agriculture, Newtown Square, PA.
4. Diffey, B. L. and P. J. Saunders (1995) Behavior outdoors and its effects on personal ultraviolet exposure rate measured using an ambulatory datalogging dosimeter. *Photochem. Photobiol.* **61**, 615–655.
5. de Gruijl, F. R. (1995) Impacts of a projected depletion of the ozone layer. *Consequences* **1**, 1–10 (http://www.gcrio.org/CONSEQUENCES/summer95/impacts.html).
6. Madronich, S. and F. R. de Gruijl (1994) Stratospheric ozone depletion between 1979 and 1992: implications for biologically active ultraviolet-B radiation and non-melanoma skin cancer incidence. *Photochem. Photobiol.* **59**, 541–546.
7. Long, C. S., A. J. Miller, H.-T. Lee, J. D. Wild, R. C. Przywarty and D. Hufford (1996) Ultraviolet index forecasts issued by the National Weather Service. *Bull. Am. Meteorol. Soc.* **77**, 729–748.
8. Parisi, A. V. and C. F. Wong (1994) A dosemetric technique for the measurement of ultraviolet radiation exposure to plants. *Photochem. Photobiol.* **60**, 470–474.
9. McKenzie, R. L., K. J. Paulin and M. Koltkamp (1997) Erythemal UV irradiances at Lauder, New Zealand: relationship between horizontal and vertical incidence. *Photochem. Photobiol.* **66**, 683–689.
10. Grant, R. H. (1998) Ultraviolet irradiance of inclined planes at the top of plant canopies. *Agric. For. Meteorol.* **89**, 281–293.
11. Grant, R. H. (1997) Biologically-active radiation in the vicinity of a single tree. *Photochem. Photobiol.* **65**, 974–982.
12. Grant, R. H. and G. M. Heisler (1996) Solar ultraviolet-B and photosynthetically-active irradiance in the urban sub-canopy. *Int. J. Biometeorol.* **39**, 201–212.
13. Brown, M. J., G. G. Parker and N. E. Posner (1994) A survey of ultraviolet-B radiation in forests. *J. Ecol.* **82**, 843–854.
14. Rowntree, R. A. (1984) Ecology of the urban forest. *Urban Ecol.* **8**, 1–12.
15. Rowntree, R. A. (1984) Forest canopy cover and land use in four eastern United States cities. *Urban Ecol.* **8**, 55–68.
16. Nowak, D. J., R. A. Rowntree, E. G. McPherson, S. M. Sisinni, E. R. Kerkmann and J. C. Stevens (1996) Measuring and analyzing urban tree cover. *Landsc. Urban Plann.* **36**, 49–57.
17. Bigelow, D. S., J. R. Slusser, A. F. Beaubien and J. H. Gibson (1998) The USDA ultraviolet radiation monitoring program. *Bull. Am. Meteorol. Soc.* **79**, 601–615.
18. Gao, W., R. H. Grant, G. M. Heisler and J. R. Slusser (2001) A geometric radiation transfer model for vegetation canopies in the UV-B. *Agron. J.* **94(3)**,
19. Gao, W. (1996) Modeling and measurement of ultraviolet irradiance in vegetation canopies. Ph.D. thesis, Purdue University.
20. Bird, R. E. (1984) A simple solar spectral model for direct-normal and diffuse horizontal irradiance. *Sol. Energy* **32**, 461–471.
21. Schippnick, P. F. and A. E. S. Green (1982) Analytical characterization of spectral irradiance in the middle ultraviolet. *Photochem. Photobiol.* **35**, 89–101.
22. Harrison, A. W. and C. A. Coombes (1988) Angular distribution of clear sky short wavelength radiance. *Sol. Energy* **40**, 57–63.
23. Grant, R. H., W. Gao and G. M. Heisler (1996) Photosynthetically-active radiation: sky radiance distributions under clear and overcast conditions. *Agric. For. Meteorol.* **82**, 267–292.
24. Grant, R. H., G. M. Heisler and W. Gao (1997) Clear sky radiance distributions in ultraviolet wavelength bands. *Theor. Appl. Climatol.* **56**, 123–135.
25. Coombes, C. A. and A. W. Harrison (1988) Angular distribution of overcast sky short wavelength radiance. *Sol. Energy* **40**, 161–166.
26. Grant, R. H., G. M. Heisler and W. Gao (1997) Ultraviolet sky radiance distributions of translucent overcast skies. *Theor. Appl. Climatol.* **58**, 129–139.
27. Steven, M. D. and M. H. Unsworth (1980) The angular distribution and interception of diffuse solar radiation below overcast skies. *Q. J. R. Meteorol. Soc.* **106**, 57–61.
28. Grant, R. H. and G. M. Heisler (1997) Obscured overcast sky radiance distributions for the ultraviolet and photosynthetically-active radiation wavebands. *J. Appl. Meteorol.* **36**, 1336–1345.
29. Gao, W., R. H. Grant and G. M. Heisler (1996) Spectral radiative properties of various tree species in ultraviolet wavelengths and the impacts on irradiance modeling and measurement. In *Proceedings of the 22nd Conference on Agricultural and Forest Meteorology*, pp. 417–418. American Meteorological Society, Boston, MA.
30. Coulson, K. L. (1975) *Solar Radiation: Diffuse Component in Solar and Terrestrial Radiation.* Academic Press, New York.

31. Latimer, J. R. (1972) *Radiation Measurement.* International Field Year for the Great Lakes Tech. Manual Series No. 2, Secretariat, Canadian National Comm. For the International Hydrological Decade, Ottawa, Canada.
32. LI-COR(1986) *LI-COR Terrestrial Radiation Sensors, Type SB. Instruction Manual.* Pub. 8609-58, LI-COR, Inc., Lincoln, NB.
33. Grant, R. H. (1996) Characterization of UVA and UVB irradiance sensor systems. In *Proceedings of the 22nd Conference on Agricultural and Forest Meteorology,* pp. 169–172. American Meteorological Society, Boston, MA.
34. McKinlay, A. F. and B. L. Diffey (1987) A reference action spectrum for ultraviolet erythema in human skin. *CIE J.* **6**, 17–22.
35. Parrish, J. A., K. F. Jaenicke and R. R. Anderson (1982) Erythema and melanogenesis action spectra of normal skin. *Photochem. Photobiol.* **36**, 187–191.
36. Diffey, B. L., C. J. Gibson, R. Haylock and A. F. McKinlay (1996) Outdoor ultraviolet exposure of children and adolescents. *Br. J. Dermatol.* **134**, 1030–1034.
37. Kimlin, M. G. and A. V. Parisi (1999) Effect of ultraviolet protective strategies on facial ultraviolet radiation exposure. In *Biometeorology and Urban Climatology at the Turn of the Millenium* (Edited by R. J. DeDear, J. D. Kalma, T. R. Oke and A. Auliciems), pp. 93–98, WCASP-50, TD-No. 1026. World Meteorological Organization.
38. Madronich, S., R. L. McKenzie, L. O. Bjorn and M. M. Caldwell (1998) Changes in biologically active ultraviolet radiation reaching the Earth's surface. *J. Photochem. Photobiol. B: Biol.* **46**, 5–19.
39. Grant, R. H., G. M. Heisler and J. Slusser (2000) Urban UV measurements: rationale for the establishment of long-term monitoring in the Baltimore ecosystem study. In *Proceedings of the 3rd Symposium on the Urban Environment,* 14–18 August 2000, pp. 195–196. American Meteorological Society, Boston, MA.